Digital Signal Processing 105 (2020) 102685

Contents lists available at ScienceDirect

Digital Signal Processing

www.elsevier.com/locate/dsp

Optimum sparse array configuration for DOA estimation on moving platforms

Guodong Qin [a,*], Moeness G. Amin [b]

[a] School of Electronic Engineering, Xidian University, Xi'an, Shaanxi 710071, China
[b] Center for Advanced Communications, Villanova University, Villanova, PA 19085, USA

ARTICLE INFO

Article history:
Available online 8 February 2020

Keywords:
Moving sparse array
Environment-dependent sparse arrays
Cramer-Rao bound
Difference coarray
Array optimization

ABSTRACT

Sparse array motion can efficiently expand the numbers of achievable degrees of freedom (DOFs) and consecutive lags, improving direction-of-arrival (DOA) estimation. Sparse arrays on a moving platform benefit from motion translation that introduces new sensor positions, which collectively with the original positions can increase the number of spatial autocorrelation lags and lead to full array augmentability. This property has been recently used for the case of environment-independent sparse array configurations, such as those defined by nested and co-prime arrays. In this paper, we consider environment-dependent sparse arrays (EDSAs) design using Cramer-Rao bound (CRB) as the metric of optimality for DOA estimation. The CRB is derived for a sparse array on a moving platform, where the number of identifiable uncorrelated sources exceeds the number of sensors. The CRB expression is used to solve for the sparse array configuration by applying the Genetic algorithm. Simulation results are provided to validate the effectiveness of the proposed EDSA design.

1. Introduction

Direction finding using multi-sensor platforms and utilizing sparse array configurations finds broad applications in many areas including communications, radar, sonar, satellite navigation, and radio telescope [1–14]. Compared with uniform arrays, sparse arrays can assume higher degree of freedoms (DOFs) and larger array aperture with the same number of sensors. Sparse array design typically seeks to position the available sensors so as to increase the number of spatial correlation lags across the array. Such objective defines what is referred to as environment-independent sparse arrays (EISAs), in which array design is not a function of the desired and interfering sources in the field of view (FOV). Examples are coprime arrays [1], minimum redundancy arrays (MRAs) [7], minimum hole arrays (MHAs) [15] and nested arrays [2]. Generally, coprime and nested arrays are designed to estimate $O(N^2)$ uncorrelated far-field narrowband sources through $O(N)$ sensors. The EISAs differ in structures and, therefore, offer different DOA estimation performance, none of which is optimum for a specific environment. Environment-dependent sparse arrays (EDSAs), on the other hand, are configured to provide optimum performance. Cramer-Rao bound (CRB) and beamforming output signal-to-noise ratio (SNR) have been considered as criteria of optimality [16–20]. Wang et al. designed the sparse arrays based on CRB [20], signal-to-interference-plus-noise ratio (SINR) [16] and SNR [17] to enhance beamforming performance.

Subspace methods for DOA estimation using EISAs utilize consecutive autocorrelation lags across the array. As such, arrays with fewer holes and longer filled coarrays are deemed to outperform those with missing and interrupted lags. Alternative DOA estimation methods based on sparse reconstructions [21–24] benefit from increased number of lags with no strict condition on consecutive arrangements. In this paper, we pursue subspace methods for EDSAs under array motions.

Fully augmented arrays can be achieved using dual or multiple frequencies, as proposed in [25,26]. For narrowband sources, missing lags can be recovered by the virtue of array motion, and under the assumption of quasi-stationarity. In essence, motion introduces a different set of autocorrelation lags depending on the array translation values and the original sensor positions. This can significantly increase the number of consecutive lags and the DOFs [27, 28]. In [29], a novel nested array is designed to obtain a hole-free coarray on a moving platform, in which case the motion amounted to a translation of half a wavelength.

In this paper, we consider sparse arrays on a moving platform similar to [29]. The CRB is used as the design objective for determining the optimum array configuration. It is directly related to the inverse of the Fisher information matrix (FIM), which contains

* Corresponding author.
E-mail addresses: gdqin@mail.xidian.edu.cn (G. Qin), moeness.amin@villanova.edu (M.G. Amin).

https://doi.org/10.1016/j.dsp.2020.102685
1051-2004/

information about all unknown parameters [30,31]. It is typically derived for the case of uniform linear arrays where the number of sources is less than the number of sensors. It also assumes the existence of the inverse of the matrix $\mathbf{A}^H\mathbf{A}$, where $\mathbf{A}$ is the so-called array manifold matrix. For the case of sparse arrays, Liu et al. [32] provided the specific expressions of the CRB when the number of sources is greater than the number of sensors, and proved that the CRB exists under the condition of the existence of the augmented coarray manifold matrix. In [20], the authors designed the sparse arrays for enhanced DOA estimation with the metric of CRB, whereas the number of sources is less than the number of sensors.

In this paper, we design optimum sparse array on a moving platform by setting the CRB to its lowest possible value under the condition that the number of sources is greater than the number of sensors. These CRB values are smaller than those rendered by employing sparse arrays which only seek to increase the number of autocorrelation lags without being cognizant of the environment. We provide numerical results that consider CRB for a high number of sources at different angles, number of snapshots, and different SNRs. It is shown that CRB values for the optimum design are not only smaller than those associated with nested and super nested arrays but also less sensitive to the source angles.

The contributions of this paper are summarized as follows. i) CRB for DOA estimation on moving platforms is derived. ii) The optimum sparse array is obtained by solving non-convex cost function based on CRB using the Genetic algorithm. iii) The optimum sparse array associated with sources in known spatial sectors is found through simulations. The results imply robustness to angle changes.

The proposed approach can be generally applied to a sensor array operating in a quasi-stationary environment, such as sonar area. Another potential application is cooperative network localization where agents communicate ranging information to improve localization accuracy [33–35]. In this case, the method proposed in this paper can be applied to design or select a optimum network under the condition of minimization of CRB.

The remainder of the paper is organized as follows. In Section 2, we describe the data model of DOA estimation on a moving platform. The nested and super nested array are reviewed in Section 3. The expressions of CRB for a sparse array on a moving platform are derived in Section 4, and the optimum array design is provided. Numerical results are presented in Section 5 to demonstrate the effectiveness of the proposed method. Section 6 concludes this paper.

Notations: We use lower-case (upper-case) bold characters to denote vectors (matrices). In particular, $\mathbf{I}_N$ denotes the $N\times N$ identity matrix. $(\cdot)^T$ and $(\cdot)^H$ respectively denote the transpose and conjugate transpose of a matrix or a vector. $(\cdot)^*$ implies complex conjugation. $\mathrm{E}(\cdot)$ is the statistical expectation operator and $\bigotimes$ denotes the Kronecker product. **Tr** is the trace of the matrix. $\mathbb{S}$ and $\mathbb{D}$ denote the sets of integers, and $\mathbb{C}$ denotes the sets of complex values. $\mathcal{CN}(\mathbf{m},\mathbf{R})$ is a complex normal distribution with mean $\mathbf{m}$ and covariance matrix $\mathbf{R}$. $rank(\mathbf{A})$ is the rank of $\mathbf{A}$, and $round(x)$ is a function which rounds x to the nearest integer.

2. Data model based on moving sparse array

Consider a sparse array with L sensors moving at a constant velocity v. The schematic is illustrated in Fig. 1, where a nested array is used as an example. The black circle and red rhombus represent the sensor positions of the original and shifted array, respectively. Denote $\mathbf{d}=[d_1,\cdots,d_L]^T$ is the positions of the array sensors, where $d_l=nd, l=1,2,\cdots,L$, with n represents an integer, $d=\lambda/2$ is the minimum inter-element spacing. The first sensor is used as a reference, i.e., $d_1=0$. The received signals from Q

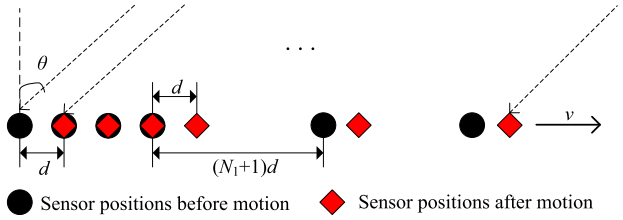

Fig. 1. DOA Estimation exploiting a moving sparse array.

far-field uncorrelated sources are described as $s_q(t)=\alpha_q s(t)$, $t=T_s,2T_s,\cdots,L_sT_s$, for $q=1,\cdots,Q$, where T_s and L_s, respectively, denote the sampling interval and the number of snapshots. α_q is the complex amplitude of the qth source, and $[\alpha_1,\alpha_2,\cdots,\alpha_Q]^T$ is assumed to be a Gaussian random vector with zero mean and covariance $diag\{p_1,p_2,\cdots,p_Q\}$, where p_q is the qth source power. The angle of arrival of the qth source is denoted as θ_q. With a relatively high speed of the array platform, the directions of the sources with respect to the sensor array can be considered fixed over a platform short translation motion. The output of the receive array, at time t, is expressed as

$$\begin{aligned}\mathbf{x}(t)&=\sum_{q=1}^{Q}s_q(t)\exp\left(-j2\pi\frac{vt\sin(\theta_q)}{\lambda}\right)\mathbf{a}(\theta_q)+\boldsymbol{\varepsilon}(t)\\&=\mathbf{A}\mathbf{s}(t)+\boldsymbol{\varepsilon}(t),\end{aligned}\tag{1}$$

where

$$\mathbf{a}(\theta_q)=\left[1,\exp(-j2\pi\frac{d_2\sin(\theta_q)}{\lambda}),\cdots,\exp(-j2\pi\frac{d_L\sin(\theta_q)}{\lambda})\right]^T$$

is the steering vector. In addition,

$$\begin{aligned}\mathbf{s}(t)=\Bigg[&s_1(t)\exp\left(-j2\pi\frac{vt\sin(\theta_1)}{\lambda}\right),\\&s_2(t)\exp\left(-j2\pi\frac{vt\sin(\theta_2)}{\lambda}\right),\cdots,\\&s_Q(t)\exp\left(-j2\pi\frac{vt\sin(\theta_Q)}{\lambda}\right)\Bigg]^T\end{aligned}\tag{2}$$

is the signal vector. $\mathbf{A}=[\mathbf{a}(\theta_1),\mathbf{a}(\theta_2),\cdots,\mathbf{a}(\theta_Q)]\in\mathbb{C}^{L\times Q}$ is the array manifold matrix, and $\boldsymbol{\varepsilon}(t)\in\mathbb{C}^{L\times 1}$ is zero-mean complex additive white Gaussian noise vector with covariance matrix $\sigma_{\boldsymbol{\varepsilon}}^2\mathbf{I}_L$. At time $t+\tau$, the output of the receive array becomes

$$\begin{aligned}\mathbf{x}(t+\tau)&=\sum_{q=1}^{Q}s_q(t+\tau)\exp\left(-j2\pi\frac{vt\sin(\theta_q)}{\lambda}\right)\\&\quad\times\exp\left(-j2\pi\frac{v\tau\sin(\theta_q)}{\lambda}\right)\mathbf{a}(\theta_q)+\boldsymbol{\varepsilon}(t+\tau)\\&=\mathbf{B}\mathbf{s}(t+\tau)+\boldsymbol{\varepsilon}(t+\tau)\end{aligned}\tag{3}$$

where

$$\mathbf{B}=[\mathbf{b}(\theta_1),\mathbf{b}(\theta_1),\cdots,\mathbf{b}(\theta_Q)]\in\mathbb{C}^{L\times Q}\tag{4}$$

with

$$\begin{aligned}\mathbf{b}(\theta_q)&=\exp\left(-j2\pi\frac{v\tau\sin(\theta_q)}{\lambda}\right)\mathbf{a}(\theta_q)\\&=\Bigg[\exp\left(-j2\pi\frac{v\tau\sin(\theta_q)}{\lambda}\right),\\&\quad\exp\left(-j2\pi\frac{(v\tau+d_2)\sin(\theta_q)}{\lambda}\right),\cdots,\end{aligned}$$

$$\exp\left(-j2\pi\frac{(v\tau+d_L)\sin(\theta_q)}{\lambda}\right)\Bigg]^T, \tag{5}$$

and

$$\mathbf{s}(t+\tau)=\Bigg[s_1(t+\tau)\exp\left(-j2\pi\frac{vt\sin(\theta_1)}{\lambda}\right), s_2(t+\tau)\exp\left(-j2\pi\frac{vt\sin(\theta_2)}{\lambda}\right),\cdots, s_Q(t+\tau)\exp\left(-j2\pi\frac{vt\sin(\theta_Q)}{\lambda}\right)\Bigg]^T. \tag{6}$$

For narrowband signals with carrier frequency f, $s_q(t+\tau)=s_q(t)\exp(j2\pi f\tau)$. Accordingly, (3) can be rewritten as

$$\mathbf{x}(t+\tau)=\exp(j2\pi f\tau)\mathbf{B}\mathbf{s}(t)+\boldsymbol{\varepsilon}(t+\tau). \tag{7}$$

By choosing $v\tau=d=\lambda/2$, the steering vector at time $t+\tau$ becomes

$$\mathbf{b}(\theta_q)=\Bigg[\exp\left(-j2\pi\frac{d\sin(\theta_q)}{\lambda}\right), \exp\left(-j2\pi\frac{(d+d_2)\sin(\theta_q)}{\lambda}\right),\cdots, \exp\left(-j2\pi\frac{(d+d_L)\sin(\theta_q)}{\lambda}\right)\Bigg]^T. \tag{8}$$

By compensating for the phase correction factor $\exp(j2\pi f\tau)$ using the technique described in [36], we attain a phase synchronized received signal vector as

$$\tilde{\mathbf{x}}(t+\tau)=\mathbf{x}(t+\tau)\exp(-j2\pi f\tau)=\mathbf{B}\mathbf{s}(t)+\tilde{\boldsymbol{\varepsilon}}(t+\tau), \tag{9}$$

where $\tilde{\boldsymbol{\varepsilon}}(t+\tau)=\exp(-j2\pi f\tau)\boldsymbol{\varepsilon}(t+\tau)$.

We obtain a synthetic array through combining equations (1) and (9). The output of the array is expressed as

$$\mathbf{y}(t)=\begin{bmatrix}\mathbf{x}(t)\\ \tilde{\mathbf{x}}(t+\tau)\end{bmatrix}=\mathbf{A}_c\mathbf{s}(t)+\begin{bmatrix}\boldsymbol{\varepsilon}(t)\\ \tilde{\boldsymbol{\varepsilon}}(t+\tau)\end{bmatrix}\in\mathbb{C}^{\tilde{L}\times 1}, \tag{10}$$

where

$$\mathbf{A}_c=[\mathbf{a}_c(\theta_1),\mathbf{a}_c(\theta_2),\cdots,\mathbf{a}_c(\theta_Q)]\in\mathbb{C}^{\tilde{L}\times Q}. \tag{11}$$

with

$$\mathbf{a}_c(\theta_q)=[\mathbf{a}^T(\theta_q),\mathbf{b}^T(\theta_q)]^T=\Big[1,u_2(\theta_q),\cdots,u_L(\theta_q),u_d(\theta_q),u_2(\theta_q)u_d(\theta_q),\cdots,u_L(\theta_q)u_d(\theta_q)\Big]^T, \tag{12}$$

where $u_l(\theta_q)=\exp\left(-j2\pi d_l\sin(\theta_q)/\lambda\right)$ and $u_d(\theta_q)=\exp\left(-j2\pi d\sin(\theta_q)/\lambda\right)$. $\tilde{L}$ is the number of sensors in the synthetic array. Note that $\tilde{L}\le 2L$ since some sensor positions before and after motion may overlap. The combined array positions before and after motion constitute the synthesized array which clearly provides higher DOF than those offered by the original array position. Let $\mathbb{S}$ and $\mathbb{S}_c$ denote the integer sets of the original array and synthetic array, respectively. According to (12), we have

$$\mathbb{S}_c=\{n\}\cup\{n+1\},\quad n\in\mathbb{S}. \tag{13}$$

If $\mathbb{D}$ and $\mathbb{D}_c$ represent the integer sets corresponding to the difference coarray of the original array and synthetic array, respectively. Then

$$\mathbb{D}=n_1-n_2,\quad n_1,n_2\in\mathbb{S},$$
$$\mathbb{D}_c=n_3-n_4,\quad n_3,n_4\in\mathbb{S}_c. \tag{14}$$

For example, if $\mathbb{S}=\{0,1,5\}$, then $\mathbb{D}=\{-5,-4,-1,0,1,4,5\}$. After array motion, $\mathbb{S}_c=\{0,1,5,6\}$. $\mathbb{D}_c=\{-6,-5,-4,-1,0,1,4,5,6\}$.

It is shown in [27] that the difference co-array of the combined two array positions consists of the difference co-array of the original array and its unit lag shifted versions along (right), $\mathbb{D}_r$, and opposite (left), $\mathbb{D}_l$, to direction of motion, i.e.,

$$\mathbb{D}_c=\mathbb{D}\cup\mathbb{D}_l\cup\mathbb{D}_r. \tag{15}$$

3. Review of the nested array and super nested array

There are two categories for the coarray configurations; one is full and the other is with holes. Most coprime arrays and MHAs belong to the former. Nested arrays, super nested arrays and MRAs are representatives of the later. Here, we review the configurations of the nested array and super nested array for better understanding of the follow on sections.

A two-level nested array consists $L=N_1+N_2$ sensors which are arranged into two uniform linear subarrays of N_1 and N_2 sensors. The sensor positions are given by [2]

$$\mathbb{P}_{n2,0}=\{nd,0\le n\le N_1-1\}\cup\{(n(N_1+1)-1)d,1\le n\le N_2\}. \tag{16}$$

For example, $L=6, N_1=N_2=3$. Then $\mathbb{S}=\{0,1,2,3,7,11\}$, $\mathbb{S}_c=\{0,1,2,3,4,7,8,11,12\}$. $\mathbb{D}=\{0,\pm1,\pm2,\cdots,\pm11\}$, $\mathbb{D}_c=\{0,\pm1,\pm2,\cdots,\pm11,\pm12\}$. Obviously, the difference coarray is hole-free whether it is considered before or after moving half a wavelength.

For a second-order super nested array with $L=N_1+N_2$ sensors, the sensor positions are given by [3]

$$\mathbb{P}_{s2,0}=\mathbb{X}_1\cup\mathbb{Y}_1\cup\mathbb{X}_2\cup\mathbb{Y}_2\cup\mathbb{Z}_1\cup\mathbb{Z}_2, \tag{17}$$

where

$$\mathbb{X}_1=\{1+2l\mid 0\le l\le A_1\}$$
$$\mathbb{Y}_1=\{(N_1+1)-(1+2l)\mid 0\le l\le B_1\}$$
$$\mathbb{X}_2=\{(N_1+1)+(2+2l)\mid 0\le l\le A_2\}$$
$$\mathbb{Y}_2=\{2(N_1+1)-(2+2l)\mid 0\le l\le B_2\}$$
$$\mathbb{Z}_1=\{l(N_1+1)\mid 2\le l\le N_2\}$$
$$\mathbb{Z}_2=\{N_2(N_1+1)-1\}.$$

The parameter A_1, B_1, A_2 and B_2 are defined as

$$(A_1,B_1,A_2,B_2)=\begin{cases}(r,r-1,r-1,r-2) & \text{if } N_1=4r,\\ (r,r-1,r-1,r-2) & \text{if } N_1=4r+1,\\ (r+1,r-1,r,r-2) & \text{if } N_1=4r+2,\\ (r,r,r,r-1) & \text{if } N_1=4r+3,\end{cases} \tag{18}$$

where r is an integer.

For example, $L=7, N_1=3, N_2=4$. Then $\mathbb{S}=\{0,2,5,7,11,14,15\}$, $\mathbb{S}_c=\{0,1,2,3,5,6,7,8,11,12,14,15,16\}$. $\mathbb{D}=\{0,\pm1,\pm2,\cdots,\pm15\}$, $\mathbb{D}_c=\{0,\pm1,\pm2,\cdots,\pm15,\pm16\}$.

4. Optimum sparse array based on Cramer-Rao low bound

Consider a real-valued random vector $\mathbf{y}$ with probability density function (pdf) $p(\mathbf{y};\boldsymbol{\beta})$, where β is a real-valued parameter vector. Assume that the $p(\mathbf{y};\boldsymbol{\alpha})$ satisfies the regularity condition $\mathrm{E}_y[(\partial/\partial\beta)\log p(\mathbf{y};\boldsymbol{\beta})]=0$. The Fisher information matrix (FIM) $\mathcal{F}(\beta)$ is defined as [32]

$$\mathcal{F}(\beta)_{ij}=-\mathrm{E}_y\left[\frac{\partial^2}{\partial\beta_i\partial\beta_j}\log p(\mathbf{y};\boldsymbol{\beta})\right]. \tag{19}$$

The CRB is given by the inverse of the FIM, if it exists, i.e.,

$$\mathrm{CRB}(\beta)=\mathcal{F}^{-1}(\beta). \tag{20}$$

The probability model with uncorrelated sources and L_s snapshots of the data observations in (10) is expressed as [32]

$$\begin{bmatrix}\mathbf{y}(T_s)\\ \mathbf{y}(2T_s)\\ \vdots\\ \mathbf{y}(L_sT_s)\end{bmatrix}\sim\mathcal{CN}\left(\mathbf{0},\begin{bmatrix}\mathbf{R_y} & \mathbf{0} & \cdots & \mathbf{0}\\ \mathbf{0} & \mathbf{R_y} & \cdots & \mathbf{0}\\ \vdots & \vdots & \ddots & \vdots\\ \mathbf{0} & \mathbf{0} & \cdots & \mathbf{R_y}\end{bmatrix}\right), \tag{21}$$

where $\mathbf{R_y}=\mathrm{E}[\mathbf{y}\mathbf{y}^H]=\mathrm{diag}\{p_1,p_2,\cdots p_Q\}\mathbf{A}_c\mathbf{A}_c^H+\sigma_{\boldsymbol{\varepsilon}}^2\mathbf{I}_{\tilde{L}}$. The parameter vector in (19) is defined as $\beta=[\theta_q,p_q,\sigma_{\boldsymbol{\varepsilon}}^2]$.

Then, the FIM $\mathcal{F}(\beta)$ is rewritten as [32]

$$\mathcal{F}(\beta)_{ij}=L_s\mathbf{Tr}\left(\mathbf{R_y^{-1}}\frac{\partial\mathbf{R_y}}{\partial\beta_i}\mathbf{R_y^{-1}}\frac{\partial\mathbf{R_y}}{\partial\beta_j}\right). \tag{22}$$

In [32], CRB is proved to exist when the rank of the augmented coarray manifold matrix (ACM) equals to $2Q+1$ for a fixed sparse array. The ACM matrix $\mathbf{A_M}$ for the motion case is defined as

$$\mathbf{A_M}=\left[\mathrm{diag}(\mathbb{D}_c)\mathbf{V}_{\mathbb{D}_c}\quad\mathbf{W}_{\mathbb{D}_c}\right], \tag{23}$$

where

$$\mathbf{V}_{\mathbb{D}_c}=[\mathbf{v}_{\mathbb{D}_c}(\theta_1)\quad\mathbf{v}_{\mathbb{D}_c}(\theta_2)\quad\ldots\quad\mathbf{v}_{\mathbb{D}_c}(\theta_Q)],$$
$$\mathbf{v}_{\mathbb{D}_c}(\theta_q)=\exp(j\pi\mathbb{D}_c\sin\theta_q), \tag{24}$$
$$\mathbf{W}_{\mathbb{D}_c}=[\mathbf{V}_{\mathbb{D}_c}\quad\mathbf{e}_0]. \tag{25}$$

Here, $\mathbf{e}_0$ is a column vector which is defined in Lemma 2 in [32]. Let η and η_c denote the numbers of unique lags of $\mathbb{D}$ and $\mathbb{D}_c$, respectively. The ACM matrix $\mathbf{A_M}$ is a $\eta_c\times(2Q+1)$ matrix for the motion case. It is a $\eta\times(2Q+1)$ matrix for the non-motion case. It was shown in [27,29] that $\mathbb{S}_c$ remains a sparse (or hole-free) array which has a higher degree of freedom than $\mathbb{S}$. Therefore, the definite condition of ACM in [32]is still suitable for the motion case, i.e., the CRB exists if and only if $rank(\mathbf{A_M})=2Q+1$.

Based on these results, we can deduce the CRB for a moving sparse array, i.e.,

$$\mathbf{CRB}(\theta)=\frac{1}{4\pi^2L_s}\left(\mathbf{G}_0^H\boldsymbol{\Pi}^{\perp}_{\mathbf{MW}_{\mathbb{D}_c}}\mathbf{G}_0\right)^{-1}, \tag{26}$$

where

$$\mathbf{G_0}=\mathbf{M}(\mathrm{diag}(\mathbb{D}_c))\times\mathbf{V}_{\mathbb{D}_c}\times(\mathrm{diag}(p_1,p_2,\ldots,p_Q)), \tag{27}$$
$$\mathbf{M}=\left(\mathbf{J}^{\mathrm{H}}(\mathbf{R}_{\mathbb{S}_c}^{\mathrm{T}}\otimes\mathbf{R}_{\mathbb{S}_c})^{-1}\mathbf{J}\right)^{\frac{1}{2}}, \tag{28}$$
$$\mathbb{S}_c=\{n\}\cup\{n+1\},\quad n\in\mathbb{S}, \tag{29}$$
$$\mathbf{R}_{\mathbb{S}_c}=\mathbf{R_y}=\mathrm{diag}\{p_1,p_2,\cdots p_Q\}\mathbf{A}_c\mathbf{A}_c^H+\sigma_{\boldsymbol{\varepsilon}}^2\mathbf{I}_{\tilde{L}}, \tag{30}$$
$$\boldsymbol{\Pi}^{\perp}_{\mathbf{MW}_{\mathbb{D}_c}}=\mathbf{I}_{\tilde{L}}-\mathbf{MW}_{\mathbb{D}_c}(\{\mathbf{MW}_{\mathbb{D}_c}\}^H\mathbf{MW}_{\mathbb{D}_c})^{-1}\{\mathbf{MW}_{\mathbb{D}_c}\}^H. \tag{31}$$

The proof can be found in Appendix A.

It can be observed from (26) that the CRB for a moving sparse array is related to the original array $\mathbb{S}$, the synthetic array $\mathbb{S}_c$, the difference coarray of the synthetic array $\mathbb{D}_c$, the DOAs θ, the number of sources Q, the number of snapshots and SNR. In order to obtain a optimum sparse array on a moving platform, we minimize the above CRB. Let A denote the array aperture, then

$$\min_{\mathbb{S}}\quad\mathbf{Tr}(\mathbf{CRB})$$
$$\text{s.t.}\quad\mathbb{S}(1)=0,\ \ \mathbb{S}(L)=A,\ \ A>L. \tag{32}$$

The objective function corresponding to the minimization of (26) is a non-convex function. We use genetic algorithms detailed in [37,38] to solve (32). The process is described in Algorithm 1. For sake of description, we let N_p, p_s, N_c and p_m denote the size of population, the selection probability, the number of crossover and the mutation probability, respectively. N_i and μ represent the number of iteration and the initial value of CRB, respectively.

For a given aperture and number of sensors, the optimum array is obtained by computing C_{A-1}^{L-2} CRBs in (26) using enumeration. For the GA method, N_i iterations are executed to obtain the optimum array. There are $N_i[N_p+round(N_p\times p_s)+4N_c+2round(N_p\times p_m)]$ CRB computations from Algorithm 1.

Algorithm 1 Genetic algorithm for array optimization.

Input: L, A, SNR,L_s, Q, θ_q, N_p, p_s,N_c, p_m, N_i, μ
Output: $\mathbb{S}$
1: Initialize the early generation of population $\mathcal{P}_0$: produce randomly the N_p unduplicated sparse array whose CRB is less than μ
2: **for all** *every iteration* $\in N_i$ **do**
3: Find the minimum of the CRB in the population, and record it and the corresponding sparse array
4: Produce the next generation of population $\mathcal{P}_k$ based on the binary tournament selection:
for every selection $\in N_p$ **do**
Choosing $N_t=round(N_p\times p_s)$ individuals from $\mathcal{P}_k$
Update $\mathcal{P}_k$ with the individual which has the minimum CRB in N_t
end
5: Execute crossover operation for updated $\mathcal{P}_k$:
for every operation $\in N_c$ **do**
Choosing 2 individuals from $\mathcal{P}_k$
Exchanging randomly the sensor positions for these 2 individuals
Update $\mathcal{P}_k$ with the exchanged 2 individuals
end
6: Execute mutation operation for updated $\mathcal{P}_k$:
for every individual $\in \mathcal{P}_k$ **do**
Produce a random number γ between zero and one
If $\gamma\le p_m$
Choosing randomly a sensor position Ξ (integer) from $2th$ to $(L-1)th$ sensor
Choosing randomly one bit from Ξ, we obtain Ξ_m
after the inverted bit is replaced the chosen bit
Update $\mathcal{P}_k$ with Ξ_m
end
end
7: **end for**
8: Find the minimum CRB for every generation, and the corresponding individual is the optimum solution $\mathbb{S}$
9: **return** $\mathbb{S}$

5. Numerical results

In this section, we examine the proposed optimum sparse array through numerical examples. We assume $A=15$, $L=7$. We consider the nested array and super nested array with the same number of the sensors and array aperture for a fair comparison. For the nested array, the sensor locations of the original array $\mathbb{S}=\{0,1,2,3,7,11,15\}$ and the respective difference coarray $\mathbb{D}=\{0,\pm1,\pm2,\cdots,\pm15\}$. After moving half wavelength, the sensor locations and the difference coarray of the synthetic array are respectively $\mathbb{S}_c=\{0,1,2,3,7,11,15,16\}$ and $\mathbb{D}_c=$

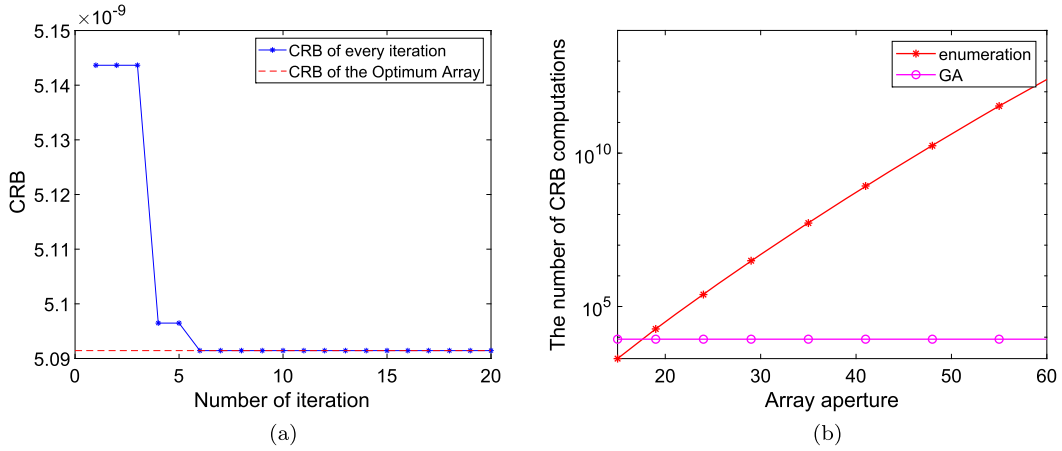

Fig. 2. The performance of GA method. (a) CRB versus the number of iteration; (b) The computational complexity.

$\{0, \pm1, \pm2, \cdots, \pm15, \pm16\}$. For the super nested array, the sensor locations of the original array $\mathbb{S} = \{0, 2, 5, 7, 11, 14, 15\}$ and the difference coarray $\mathbb{D} = \{0, \pm1, \pm2, \cdots, \pm15\}$. After array motion of half a wavelength, it has the same sensor locations and the difference coarray as those of the nested array. We consider $Q = 9$ equal-power sources located at $0.5 \sin\theta_q = -0.49 + 0.9(q-1)/Q$.

5.1. The performance of GA method

In the first example, we examine the performance of GA method. Let SNR = 0dB, the number of snapshots is set as 10000. $N_p = 50$, $p_s = 0.2$, $N_c = 90$, $p_m = 0.1$, $N_i = 20$. The other parameters are the same as above. The computation complexity is presented in Fig. 2(a). It is obvious that the GA method converges when the number of iteration is 6. At this time, the CRB of the optimum array is the same as that of the optimum array obtained by enumeration. In Fig. 2 (b), we plot the number of CRB computations versus the array aperture. The array aperture varies from 15 to 60. It can be seen from the figure that GA method has a higher computation complexity than the enumeration when the array aperture is relatively small. Accordingly, the GA method has advantages under the condition of large aperture.

5.2. The CRB of the optimum array for different snapshots

In the second example, we let SNR = 0dB, the number of snapshots varies from 10 to 10000. The simulation results are shown in Fig. 3. From the figure, the CRB decreases with the number of snapshots. For the same number of sensors and array aperture, the optimum array has the lowest CRB which is superior to both the super nested array and the nested array. The sensor locations of the optimum array before and after motion, the difference coarray of the synthetic array are presented in Fig. 4 (a)-(g). It is noted that the optimum array is independent of the number of snapshots. This is because the CRB is inverse proportional to the number of the snapshots, which can be seen in (26). The nested array and the super nested array, as well as their difference co-arrays are shown in Fig. 4 (h). We observe that there are only 4 common sensor positions (marked with green color) between the nested array and the optimum array, underscoring the difference in configurations. The same overlapping occurs between the super nested array and the optimum array.

5.3. The CRB of the optimum array for different SNRs

In the third example, we let $L_s = 1000$, the SNR varies from -20 dB to 30 dB. The simulation results are shown in Fig. 5. Similar

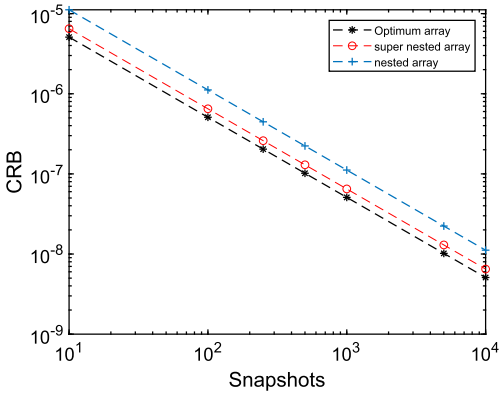

Fig. 3. CRB versus the number of snapshots.

to the second example, CRB decreases with the increments of SNR. For the same number of sensors and array aperture, the optimum array has the lowest CRB which is superior to the super nested array and the nested array. The sensor locations of the optimum array before and after motion as well as the difference coarray of the synthetic array are presented in Fig. 6 (a)-(k). The difference is that the optimum array configuration changes with SNR. From Fig. 6 (l), when considering the employed values of SNR, there are 6 overlapping sensors between the nested array and the optimum array, which is same as that between the super nested array and the optimum array.

5.4. The CRB of the optimum array for angular increment

In practical scenarios, the source angular directions are not known a priori and cannot, therefore, be used to derive CRB. However, the sources DOAs may be known within defined spatial sectors. We consider CRB-based optimum array design for different source angles. We use $Q = 9$ sources uniformly distributed from -60^o to 60^o and SNR=5 dB. Each source angle is allowed to change around its center value from -10^o to 10^o with an increment of 2 degrees. The source center angles are -60^o, -45^o, -30^o, -15^o, 0^o, 15^o, 30^o, 45^o and 60^o. This arrangement generates 11 sets with 11 CRB values corresponding to potentially 11 different sparse array configurations. The results of CRB versus angular increment are presented in Fig. 7 and 9. Each increment describes one set of sources or one environment, with zero increment corresponds to the center angles. CRB-based optimization over the 11 source sets only yields two optimum arrays, optimum array 1 and optimum array 2, which are shown in Fig. 8. Only one sensor is different in the two arrays. Clearly, optimum array 1 and optimum array 2 have a

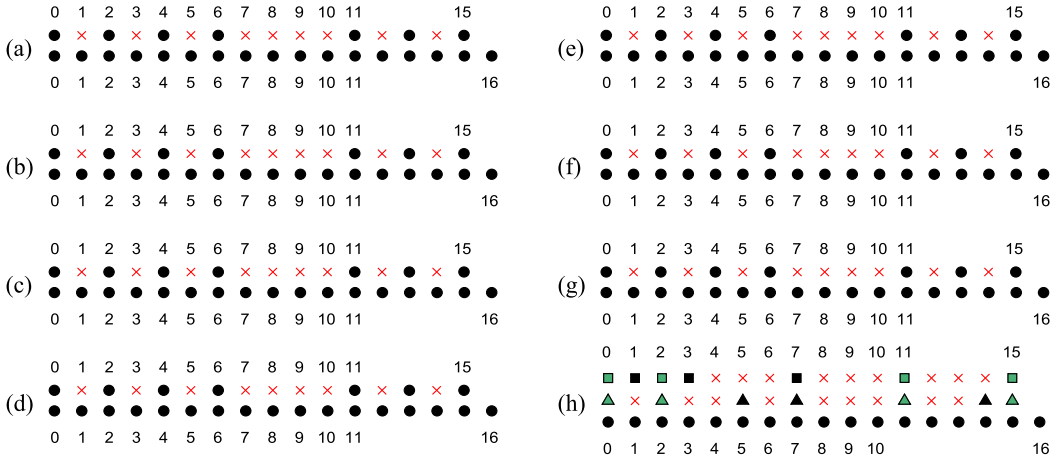

Fig. 4. The optimum array (the first line) and the non-negative parts of the difference coarray (the second line) for every snapshot in Fig. 3. (a) $L_s = 10$, (b) $L_s = 100$, (c) $L_s = 250$, (d) $L_s = 500$, (e) $L_s = 1000$, (f) $L_s = 5000$, (g) $L_s = 10000$, (h) □: the nested array; △: the super nested array; •: the difference coarray. (•:sensors; ×:holes; green:overlapping sensors).

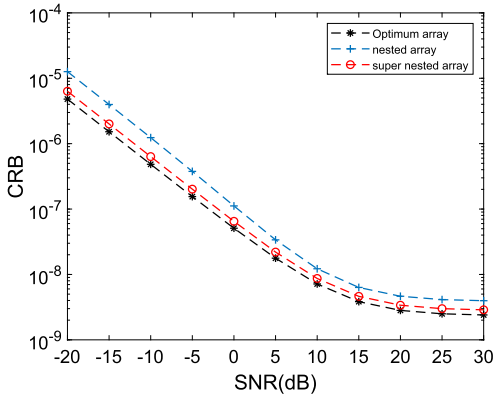

Fig. 5. CRB versus SNR.

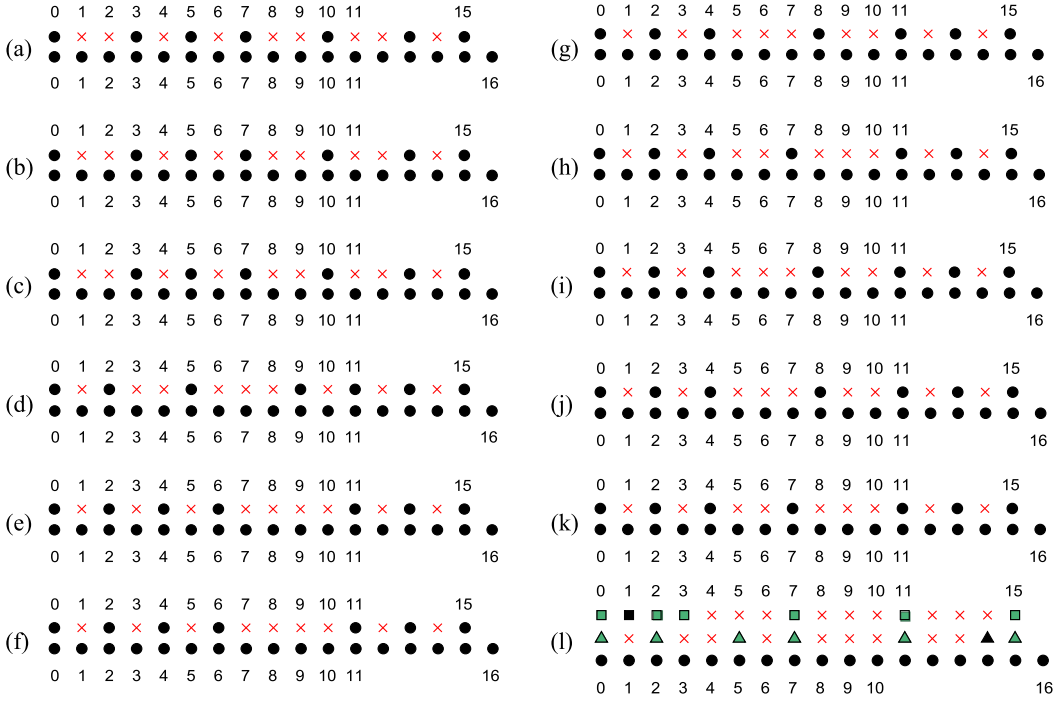

Fig. 6. The optimum array (the first line) and the non-negative parts of the difference coarray (the second line) for every SNR in Fig. 5. (a) SNR = −20 dB, (b) SNR = −15 dB, (c) SNR = −10 dB, (d) SNR = −5 dB, (e) SNR = 0 dB, (f) SNR = 5 dB, (g) SNR = 10 dB, (h) SNR = 15 dB, (i) SNR = 20 dB, (j) SNR = 25 dB, (k) SNR = 30 dB.

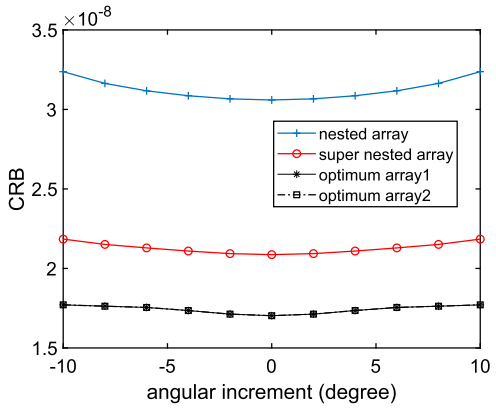

Fig. 7. CRB versus SNR.

lower bound than those of the nested and the super nested arrays, and the bound is also robust to changes in angle, as can be seen in Fig. 9. From the figure, optimum array 1 and optimum array 2 have the same performance. The difference between the highest and lowest values of the CRB for the optimum arrays is 0.068 $\times 10^{-8}$, whereas it is 0.097 $\times 10^{-8}$ for the super nested array. The nested array has the largest difference value, which implies that it is less robust than the other arrays.

6. Conclusion

In this paper, we considered sparse array design for moving platforms where the observations are collected at two instants of time separated by a motion of half a wavelength. The design objective is the minimization of CRB of the parameters underlying DOA

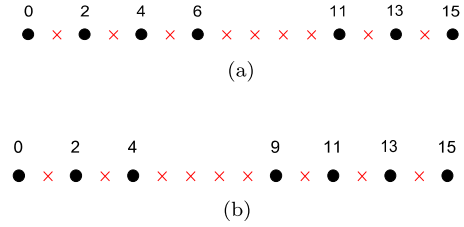

Fig. 8. The optimum sparse arrays for mismatched DOA. (a) Optimum array1; (b) Optimum array2.

estimation problems. The paper focused on narrowband uncorrelated sources and dealt with the case where the number of sources exceeds the number of sensors. The CRB of the obtained sparse array configuration is less than that of environment-independent sparse array considered, namely, the nested array and super nested array, under the conditions of the same array aperture and the same number of sensors. Although the optimum array differs with SNR, it remains fully augmented.

7. Acknowledgments

This work was supported by the National Natural Science Foundation of China (61805189).

Declaration of competing interest

The authors declare that they have no known competing financial interests or personal relationships that could have appeared to influence the work reported in this paper.

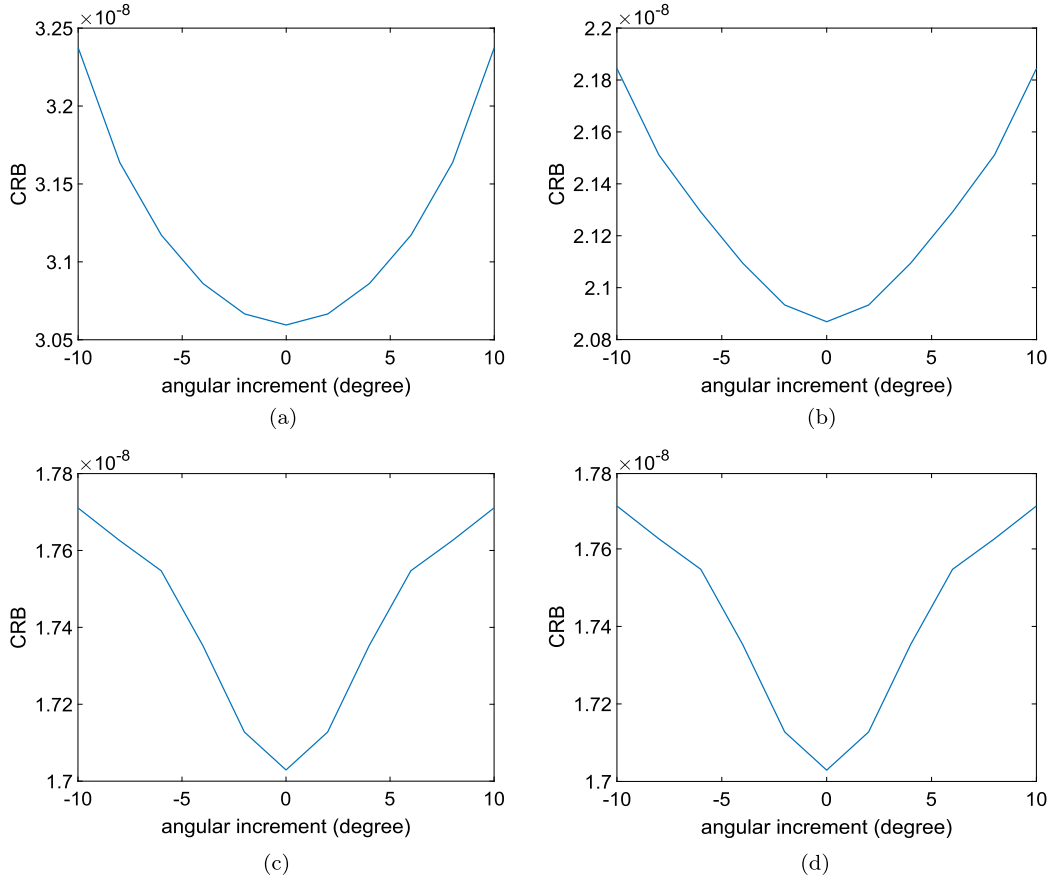

Fig. 9. The CRB of sparse array versus angle bias. (a) The nested array; (b) The super nested array; (c) The optimum array1; (d) The optimum array2.

Appendix A. Proof of CRB

If (19) is nonsingular, the CRB can be expressed as [32,39]

$$\mathbf{CRB}(\theta)=\frac{1}{L_s}\left(\mathbf{G}^H\mathbf{\Pi}_{\mathbf{\Delta}}^{\perp}\mathbf{G}\right)^{-1}, \tag{A.1}$$

where $\mathbf{G}=(\mathbf{R}_{\mathbf{y}}^T\otimes\mathbf{R}_{\mathbf{y}})^{-\frac{1}{2}}\left[\frac{\partial\mathbf{r}_{\mathbf{y}}}{\partial\theta_1}\cdots\frac{\partial\mathbf{r}_{\mathbf{y}}}{\partial\theta_Q}\right]$, $\Delta=(\mathbf{R}_{\mathbf{y}}^T\otimes\mathbf{R}_{\mathbf{y}})^{-\frac{1}{2}}\times\left[\frac{\partial\mathbf{r}_{\mathbf{y}}}{\partial p_1}\cdots\frac{\partial\mathbf{r}_{\mathbf{y}}}{\partial p_Q}\frac{\partial\mathbf{r}_{\mathbf{y}}}{\partial\sigma_{\boldsymbol{\varepsilon}}^2}\right]$. $\Pi_{\Delta}^{\perp}=\mathbf{I}-\Delta(\Delta^H\Delta)^{-1}\Delta^H$ is the orthogonal projection onto the null space of Δ^H. $\mathbf{r}_{\mathbf{y}}=\mathrm{vec}(\mathbf{R}_{\mathbf{y}})$, where $\mathrm{vec}(\cdot)$ is the vectorization. Using the binary matrix $\mathbf{J}$ defined in the Appendix B in [32], we can obtain

$$\mathbf{a}_c^*(\theta_i)\otimes\mathbf{a}_c(\theta_i)=\mathbf{J}\mathbf{V}_{\mathbb{D}_c}. \tag{A.2}$$

The vector $\mathbf{r}_{\mathbf{y}}$ is rewritten as

$$\mathbf{r}_{\mathbf{y}}=\mathbf{J}(\mathbf{V}_{\mathbb{D}_c}\mathbf{p}+\sigma_{\boldsymbol{\varepsilon}}^2\mathbf{e}_{\mathbf{0}})=\mathbf{J}\mathbf{W}_{\mathbb{D}_c}\begin{bmatrix}\mathbf{p}\\ \sigma_{\boldsymbol{\varepsilon}}^2\end{bmatrix} \tag{A.3}$$

where $\mathbf{p}=[p_1,\cdots,p_Q]^T$.

Combining (A.3) and $\mathbf{G}$ yields

$$\mathbf{G}=j2\pi(\mathbf{R}_{\mathbf{y}}^T\otimes\mathbf{R}_{\mathbf{y}})^{-\frac{1}{2}}\mathbf{J}(\mathrm{diag}(\mathbb{D}_c))\mathbf{V}_{\mathbb{D}_c}\mathbf{P}, \tag{A.4}$$

where $\mathbf{P}=\mathrm{diag}(p_1,\cdots,p_Q)$. Similarly, we can rewrite Δ as

$$\mathbf{\Delta}=(\mathbf{R}_{\mathbf{y}}^T\otimes\mathbf{R}_{\mathbf{y}})^{-\frac{1}{2}}\mathbf{J}\mathbf{W}_{\mathbb{D}_c}. \tag{A.5}$$

Substituting (A.4) and (A.5) into (A.1) yields

$$\begin{aligned}
&\mathbf{CRB}(\theta)\\
&=\frac{1}{4\pi^2L_s}\left(\mathbf{G}^H\mathbf{\Pi}_{\mathbf{\Delta}}^{\perp}\mathbf{G}\right)^{-1} \qquad (A.6)\\
&=\frac{1}{4\pi^2L_s}\mathbf{P}^H\mathbf{V}_{\mathbb{D}_c}^H(\mathrm{diag}(\mathbb{D}_c))^H\cdot\\
&\quad\left[\mathbf{J}^H(\mathbf{R}_{\mathbf{y}}^T\otimes\mathbf{R}_{\mathbf{y}})^{-\frac{1}{2}}\Pi^{\perp}_{(\mathbf{R}_{\mathbf{y}}^T\otimes\mathbf{R}_{\mathbf{y}})^{-\frac{1}{2}}\mathbf{J}\mathbf{W}_{\mathbb{D}_c}}(\mathbf{R}_{\mathbf{y}}^T\otimes\mathbf{R}_{\mathbf{y}})^{-\frac{1}{2}}\mathbf{J}\right]\cdot\\
&\quad(\mathrm{diag}(\mathbb{D}_c))\mathbf{V}_{\mathbb{D}_c}\mathbf{P}\\
&=\frac{1}{4\pi^2L_s}\mathbf{P}^H\mathbf{V}_{\mathbb{D}_c}^H(\mathrm{diag}(\mathbb{D}_c))^H\cdot\\
&\quad\left[\mathbf{M}^H\mathbf{M}-\mathbf{M}^H(\mathbf{M}\mathbf{W}_{\mathbb{D}_c})[(\mathbf{M}\mathbf{W}_{\mathbb{D}_c})^H(\mathbf{M}\mathbf{W}_{\mathbb{D}_c})]^{-1}[(\mathbf{M}\mathbf{W}_{\mathbb{D}_c})^H\mathbf{M}\right]\cdot\\
&\quad(\mathrm{diag}(\mathbb{D}_c))\mathbf{V}_{\mathbb{D}_c}\mathbf{P}\\
&=\frac{1}{4\pi^2L_s}\left(\mathbf{G}_0^H\mathbf{\Pi}^{\perp}_{\mathbf{M}\mathbf{W}_{\mathbb{D}_c}}\mathbf{G}_0\right)^{-1},
\end{aligned}$$

where $\mathbf{G}_0=\mathbf{M}(\mathrm{diag}(\mathbb{D}_c))\mathbf{V}_{\mathbb{D}_c}\mathbf{P}$, $\mathbf{M}=\left(\mathbf{J}^{\mathrm{H}}(\mathbf{R}_{\mathbb{S}_c}^{\mathrm{T}}\otimes\mathbf{R}_{\mathbb{S}_c})^{-1}\mathbf{J}\right)^{\frac{1}{2}}$.

References

[1] P.P. Vaidyanathan, P. Pal, Sparse sensing with co-prime samplers and arrays, IEEE Trans. Signal Process. 59 (2) (2011) 573–586, https://doi.org/10.1109/TSP.2010.2089682.

[2] P. Pal, P.P. Vaidyanathan, Nested arrays: a novel approach to array processing with enhanced degrees of freedom, IEEE Trans. Signal Process. 58 (8) (2010) 4167–4181, https://doi.org/10.1109/TSP.2010.2049264.

[3] C.-L. Liu, P.P. Vaidyanathan, Super nested arrays: linear sparse arrays with reduced mutual coupling – part I: fundamentals, IEEE Trans. Signal Process. 64 (15) (2016) 3997–4012, https://doi.org/10.1109/TSP.2016.2558159.

[4] C. Liu, P.P. Vaidyanathan, Remarks on the spatial smoothing step in coarray music, IEEE Signal Process. Lett. 22 (9) (2015) 1438–1442, https://doi.org/10.1109/LSP.2015.2409153.

[5] S. Qin, Y.D. Zhang, M.G. Amin, Generalized coprime array configurations for direction-of-arrival estimation, IEEE Trans. Signal Process. 63 (6) (2015) 1377–1390, https://doi.org/10.1109/TSP.2015.2393838.

[6] Z. Tan, A. Nehorai, Sparse direction of arrival estimation using co-prime arrays with off-grid targets, IEEE Signal Process. Lett. 21 (1) (2014) 26–29, https://doi.org/10.1109/LSP.2013.2289740.

[7] A. Moffet, Minimum-redundancy linear arrays, IEEE Trans. Antennas Propag. 16 (2) (1968) 172–175, https://doi.org/10.1109/TAP.1968.1139138.

[8] W. Wang, S. Ren, Z. Chen, Unified coprime array with multi-period subarrays for direction-of-arrival estimation, Digit. Signal Process. 74 (2018) 30–42, https://doi.org/10.1016/j.dsp.2017.11.015.

[9] M. Yang, L. Sun, X. Yuan, B. Chen, A new nested MIMO array with increased degrees of freedom and hole-free difference coarray, IEEE Signal Process. Lett. 25 (1) (2018) 40–44, https://doi.org/10.1109/LSP.2017.2766294.

[10] K. Adhikari, J.R. Buck, K.E. Wage, Extending coprime sensor arrays to achieve the peak side lobe height of a full uniform linear array, EURASIP J. Adv. Signal Process. 2014 (1) (2014) 148, https://doi.org/10.1186/1687-6180-2014-148.

[11] X. Yuan, Coherent source direction-finding using a sparsely-distributed acoustic vector-sensor array, IEEE Trans. Aerosp. Electron. Syst. 48 (3) (2012) 2710–2715, https://doi.org/10.1109/TAES.2012.6237621.

[12] B. Liao, S. Chan, Direction-of-arrival estimation in subarrays-based linear sparse arrays with gain/phase uncertainties, IEEE Trans. Aerosp. Electron. Syst. 49 (4) (2013) 2268–2280, https://doi.org/10.1109/TAES.2013.6621815.

[13] F. Wen, J. Shi, Z. Zhang, Joint 2d-dod, 2d-doa and polarization angles estimation for bistatic emvs-mimo radar via parafac analysis, IEEE Trans. Veh. Technol. (2019), https://doi.org/10.1109/TVT.2019.2957511.

[14] J. Shi, G. Hu, X. Zhang, F. Sun, Sparsity-based doa estimation of coherent and uncorrelated targets with flexible mimo radar, IEEE Trans. Veh. Technol. 68 (6) (2019) 5835–5848, https://doi.org/10.1109/TVT.2019.2913437.

[15] D.A. Linebarger, I.H. Sudborough, I.G. Tollis, Difference bases and sparse sensor arrays, IEEE Trans. Inf. Theory 39 (2) (1993) 716–721, https://doi.org/10.1109/18.212309.

[16] X. Wang, M. Amin, X. Cao, Analysis and design of optimum sparse array configurations for adaptive beamforming, IEEE Trans. Signal Process. 66 (2) (2018) 340–351, https://doi.org/10.1109/TSP.2017.2760279.

[17] X. Wang, M. Amin, X. Wang, X. Cao, Sparse array quiescent beamformer design combining adaptive and deterministic constraints, IEEE Trans. Antennas Propag. 65 (11) (2017) 5808–5818, https://doi.org/10.1109/TAP.2017.2751672.

[18] X. Wang, E. Aboutanios, M. Trinkle, M.G. Amin, Reconfigurable adaptive array beamforming by antenna selection, IEEE Trans. Signal Process. 62 (9) (2014) 2385–2396, https://doi.org/10.1109/TSP.2014.2312332.

[19] X. Wang, M. Amin, Design of optimum sparse array for robust MVDR beamforming against DOA mismatch, in: 2017 IEEE 7th International Workshop on Computational Advances in Multi-Sensor Adaptive Processing (CAMSAP), 2017, pp. 1–5.

[20] X. Wang, E. Aboutanios, M.G. Amin, Adaptive array thinning for enhanced DOA estimation, IEEE Signal Process. Lett. 22 (7) (2015) 799–803, https://doi.org/10.1109/LSP.2014.2370632.

[21] Y.D. Zhang, M.G. Amin Himed, Sparsity-based DOA estimation using co-prime arrays, in: Proc. IEEE Int. Conf. Acoustics, Speech and Signal Process, ICASSP, Vancouver, CA, 2013, pp. 3967–3971.

[22] Z. Yang, L. Xie, Exact joint sparse frequency recovery via optimization methods, IEEE Trans. Signal Process. 64 (19) (2016) 5145–5157, https://doi.org/10.1109/TSP.2016.2576422.

[23] Y. Gu, Y.D. Zhang, N.A. Goodman, Optimized compressive sensing-based direction-of-arrival estimation in massive MIMO, in: Proc. IEEE Int. Conf. Acoustics, Speech and Signal Process, ICASSP, New Orleans, US, 2017, pp. 3181–3185.

[24] C. Zhou, Y. Gu, X. Fan, Z. Shi, G. Mao, Y.D. Zhang, Direction-of-arrival estimation for coprime array via virtual array interpolation, IEEE Trans. Signal Process. 66 (22) (2018) 5956–5971, https://doi.org/10.1109/TSP.2018.2872012.

[25] E. BouDaher, Y. Jia, F. Ahmad, M.G. Amin, Multi-frequency co-prime arrays for high-resolution direction-of-arrival estimation, IEEE Trans. Signal Process. 63 (14) (2015) 3797–3808, https://doi.org/10.1109/TSP.2015.2432734.

[26] S. Qin, Y.D. Zhang, M.G. Amin, B. Himed, DOA estimation exploiting a uniform linear array with multiple co-prime frequencies, Signal Process. 130 (2017) 37–46.

[27] G. Qin, M.G. Amin, Y.D. Zhang, DOA estimation exploiting sparse array motions, IEEE Trans. Signal Process. 67 (11) (2019) 3013–3027, https://doi.org/10.1109/TSP.2019.2911261.

[28] G. Qin, M.G. Amin, Y.D. Zhang, Analysis of coprime arrays on moving platform, in: ICASSP 2019 - 2019 IEEE International Conference on Acoustics, Speech and Signal Processing (ICASSP), 2019, pp. 4205–4209.

[29] G. Qin, Y.D. Zhang, M.G. Amin, DOA estimation exploiting moving dilated nested arrays, IEEE Signal Process. Lett. 26 (3) (2019) 490–494, https://doi.org/10.1109/LSP.2019.2894467.

[30] P. Stoica, A. Nehorai, Music, maximum likelihood, and Cramer-Rao bound, IEEE Trans. Acoust. Speech Signal Process. 37 (5) (1989) 720–741, https://doi.org/10.1109/29.17564.

[31] P. Stoica, A. Nehorai, Performance study of conditional and unconditional direction-of-arrival estimation, IEEE Trans. Acoust. Speech Signal Process. 38 (10) (1990) 1783–1795, https://doi.org/10.1109/29.60109.

[32] C.-L. Liu, P. Vaidyanathan, Cramer-Rao bounds for coprime and other sparse arrays, which find more sources than sensors, Digit. Signal Process. 61 (2017), https://doi.org/10.1016/j.dsp.2016.04.011.

[33] W. Yuan, N. Wu, B. Etzlinger, Y. Li, C. Yan, L. Hanzo, Expectation–maximization-based passive localization relying on asynchronous receivers: centralized versus distributed implementations, IEEE Trans. Commun. 67 (1) (2019) 668–681, https://doi.org/10.1109/TCOMM.2018.2866478.
[34] W. Yuan, N. Wu, Q. Guo, X. Huang, Y. Li, L. Hanzo, TOA-based passive localization constructed over factor graphs: a unified framework, IEEE Trans. Commun. 67 (10) (2019) 6952–6965, https://doi.org/10.1109/TCOMM.2019.2930517.
[35] F. Meyer, O. Hlinka, H. Wymeersch, E. Riegler, F. Hlawatsch, Distributed localization and tracking of mobile networks including noncooperative objects, IEEE Trans. Signal Inf. Process. Netw. 2 (1) (2016) 57–71, https://doi.org/10.1109/TSIPN.2015.2511920.
[36] S. Stergiopoulos, E.J. Sullivan, Extended towed array processing by an overlap correlator, J. Acoust. Soc. Am. 86 (1) (1989) 158–171, https://doi.org/10.1121/1.398335.
[37] K. Lu, G. Zeng, J. Chen, W. Peng, Z. Zhang, Y. Dai, Q. Wu, Comparison of binary coded genetic algorithms with different selection strategies for continuous optimization problems, in: 2013 Chinese Automation Congress, 2013, pp. 364–368.
[38] Shinn-Ying Ho, Li-Sun Shu, Jian-Hung Chen, Intelligent evolutionary algorithms for large parameter optimization problems, IEEE Trans. Evol. Comput. 8 (6) (2004) 522–541, https://doi.org/10.1109/TEVC.2004.835176.
[39] P. Stoica, E.G. Larsson, A.B. Gershman, The stochastic crb for array processing: a textbook derivation, IEEE Signal Process. Lett. 8 (5) (2001) 148–150, https://doi.org/10.1109/97.917699.

Guodong Qin received the M.Sc. and Ph.D. degrees from Xidian University, Xi'an, China, in 2006 and 2009, both in electrical engineering. Since 2010, he has been with the Faculty of the School of Electronic Engineering, Xidian University. From 2017 to 2018, he was a Visiting Research Scholar with the Center for Advanced Communications, Villanova University, Villanova, PA, USA. His research interests include direction-of-arrival estimation, sparse array and signal processing, and statistical signal processing.

Moeness G. Amin received the B.Sc. degree from Cairo University, Cairo, Egypt, in 1976, the M.Sc. degree from the University of Petroleum and Minerals, Dhahran, Saudi Arabia, in 1980, and the Ph.D. degree from the University of Colorado, Boulder, CO, USA in 1984, all in electrical engineering. He is currently the Director of the Center for Advanced Communications, Villanova University, Villanova, PA, USA. He is the recipient of the 2017 Fulbright Distinguished Chair, the 2016 Alexander von Humboldt Research Award, the 2016 Institution of Engineering and Technology Achievement Medal, the 2014 IEEE Signal Processing Society Technical Achievement Award, the 2009 European Association for Signal Processing Technical Achievement Award, the 2015 IEEE Aerospace and Electronic Systems Society Warren White Award for Excellence in Radar Engineering, and the IEEE Third Millennium Medal. He is a Fellow of the International Society of Optical Engineering, the Institute of Engineering and Technology, and the European Association for Signal Processing.